Numerical simulation for vertical take-off and landing unmanned aerial vehicles (VTOL-UAV) using Virtual Blade Model (VBM)

Conference Paper · January 2018

3 authors:

Khanh Nguyen
Konkuk University
15 PUBLICATIONS   **80** CITATIONS

SEE PROFILE

Hong-Hieu Le
Ho Chi Minh City University of Technology
25 PUBLICATIONS   **72** CITATIONS

SEE PROFILE

Nguyễn Ngọc Hiền
Can Tho University of Medicine and Pharmacy
17 PUBLICATIONS   **400** CITATIONS

SEE PROFILE

NUMERICAL SIMULATION FOR VERTICAL TAKE-OFF AND LANDING UNMANNED AERIAL VEHICLES (VTOL – UAV) USING VIRTUAL BLADE MODEL

NGUYEN Khanh [1], LE Thi Hong Hieu [1], NGUYEN Ngoc Hien [2]
[1] Ho Chi Minh City University of Technology, Viet Nam
[2] RMIT University, Australia
Email: g1301784@hcmut.edu.vn

ABSTRACT

This paper presents a numerical approach to study aerodynamic characteristics of a vertical take-off and landing unmanned aerial vehicles (VTOL-UAV) using the virtual blade model of the *rotorDisk* library in OpenFOAM. The UAV addressed in this paper is a tricopter with the tricopter' arms: 1m in size equipped with three commercial propellers typed XOAR PJP-T-L 12x45 with two blades, 12 inch diameter (0.3m) and 4.5 inch pitch (0.1125m). The Virtual Blade Model (VBM) is employed to study the interactive effects between the rotors and airflow, which embedded in the Reynolds-Averaged Navier-Stokes (RANS) simulation. The salient advantage of this method is that it yields good results within reasonable computational time by representing the process of rotor modelling with basic geometrical parameters and meshing requirement.

To perform the simulation, a complete description of the propeller's characteristics is required. A steady, incompressible solver with K-ω SST turbulence model is set up. By varying inlet velocities, the model is able to study different flight regimes from hovering to vertical climbing. The entire flow fields reflecting the interaction between rotors and airflow can be discussed both in qualitatively and quantitatively. The simulated results of forces and pitching moments of the propellers are verified against the manufacturer's specification as well as the traditional Blade Element Momentum Theory (BEMT).

KEYWORDS: *tricopter, propeller's characteristics, VBM, RANS, OpenFOAM.*

1. INTRODUCTION

Unmanned aerial vehicles (UAVs) have reached wide applications in the military and civilian purposes. Thanks to the mobility, UAVs can perform various challenging activities in an efficient way. They have come to aid in various economic activities, besides search and rescue tasks or monitoring operations. In this study, we focus on the rotor aerodynamics of the tricopter design illustrated in Fig 1.

The simulation of airflow through tricopter rotors is conducted by using the *rotorDisk* library in the open source software OpenFOAM. Unlike fixed-wing airplanes, the tricopter has a problem when simulating the flow through the propeller. Currently, there are several methods for solving this problem in numerical approach with steady and compressible flow condition such as the multiple reference frame method (MRF), the single reference frame method (SRF), the virtual blade model method (VBM) (Leishman, 2000), (Antonio Filippone, 2003), etc. In this paper, the VBM is employed to model a simplified rotor blade and calculate the propeller's aerodynamic properties.

The VBM method was originally introduced by (Zori et al, 1995) using traditional Blade Element Theory (BET) for calculating the resultant lift and pitching moment at each blade element by identifying velocity distribution along the rotor blade. VBM requires a look-up table of lift and drag values by attacking angle. However, unlike other methods, VBM does not require an actual three-dimensional rotor model. It requires only the basic geometric characteristics of the propeller for a simplified rotor model. As a result, the computational time is shortened because of the reduced number of grid cells.

Currently, the numerical analysis of helicopter's rotor is performed by standard CFD solvers (OpenFOAM, ANSYS Fluent, etc.,) with various computational modules, but the VBM module has enjoyed some success in recent years such as Wahono (2013) and Antonio (2003). In these papers, the authors used the VBM module for simulating certain flight regimes of the helicopter rotor blade. On the other hand, another module combined both the VBM and the Blade Deformation Solver (BDS) to include the effect of blade deformation or flap-torsion

kinematic coupling on the final rotor characteristics (Sieradzki, 2016).
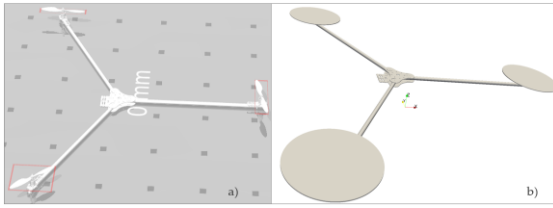

Fig 1. a) The tricopter model – b) Virtual blade geometries

Several papers (Wahono, 2013), (Antonio Filippone, 2003), (Sieradzki, 2016) and (Tri, 2015) have presented different domain shapes and sizes for each flight condition. For forward flight cases, the domain has a rectangular shape while for hovering it is a cylinder

The aim of this research is to combine the VBM and the RANS solvers in OpenFOAM to study the flow characteristics of the tricopter under different axial flight conditions. The remaining of this paper is organized in the following. In Section 2, the implementation of the rotor model in OpenFOAM is presented. It includes the problem identification, meshing process, propeller's characteristics, turbulence model, and boundary conditions. Then, the numerical results are discussed carefully in Section 3. Finally, some conclusions and recommendations are addressed in Section 4.

2. IMPLEMENTATION OF ROTOR MODEL IN OPENFOAM

2.1 Problem specification

The commercial propeller typed XOAR PJP-T-L 12x45 (1245) with two blades, RC Carbon fiber (propeller with brushless motor) is chosen for the propulsion system of the tricopter (Fig 2).

Fig 2. XOAR PJP –T –L 12x45

The tricopter is chosen to simulate the aerodynamic properties and the interaction between the rotors and the flow field around the tricopter. The general structure of the tricopter is shown in Fig 1 with the airframe comprises of three arms and three rotors. The arm's length is approximately 1 m (R_{ref} = 1m) and the rotor radius of 0.15 m. In this paper, certain axial climb regimes are investigated. Computational resources are used for total execution time:

• Laptop
Memory: 16 GB
Processor: Intel® Core i7-7700HQ CPU @ 2.8GHz x 8
• The High Performance Computing system of HCMUT
Memory: 128 GB
Processor: Intel® Xeon® CPU E5-2680v3 @2.5GHz x 48

2.2 Geometry and mesh configuration

In this paper, we choose two tools for the mesh generation. Firstly, Salome software is used for meshing the cylinder domain (Fig 3), which is defined as a background hexahedral mesh. Then, the snappyHexMesh – a refining hexahedral meshing tool is used for the tricopter and three rotor discs (Fig 4).
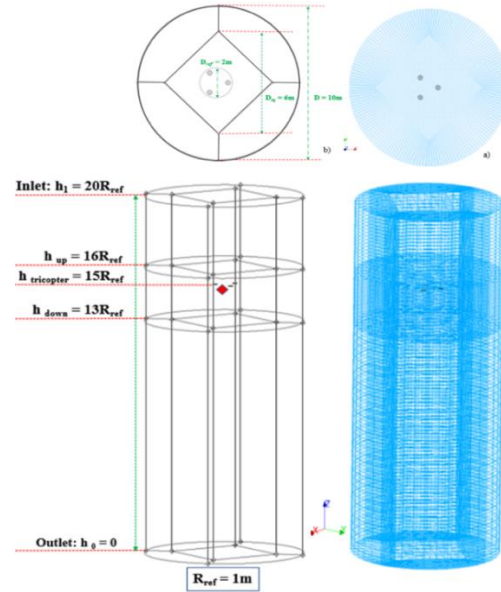

Fig 3. Domain and size (Salome software)

In VBM module, rotor disc is required for one-cell thickness approximate 2% of rotor radius (0.3 mm).
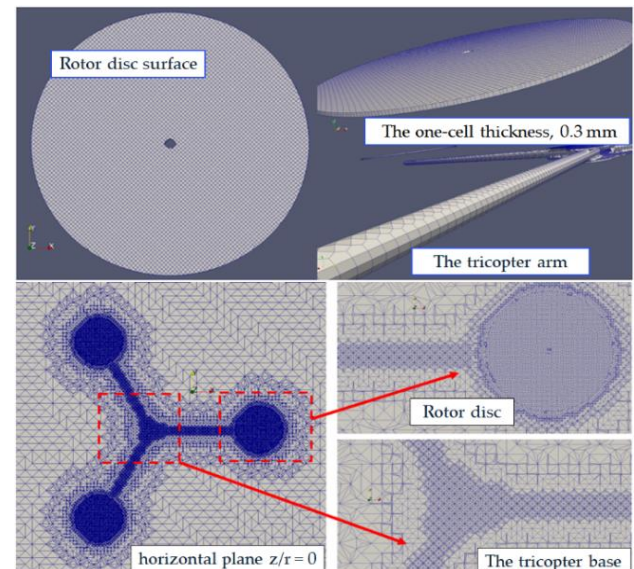

Fig 4. Mesh configuration (snappyHexMesh)

2.3 Description of rotor blade properties

This section presents a process of creating a simplified rotor blade model such as blade geometrical angle, distribution of linear taper ratio along the rotor length as well as the influence of local linear velocities on the airfoil selection. Propeller PJP-T-L 1245 with 12 inch

diameter and 4.5 inch pitch is declared as inputs for the different taking-off and landing scenerios. In general, for the case of fixed-pitch propellers, the blade geometrical angle consists of only the twist angle distributed from the root to tip. Fig 5 shows 6 spans with different slopes of twist angle distribution.

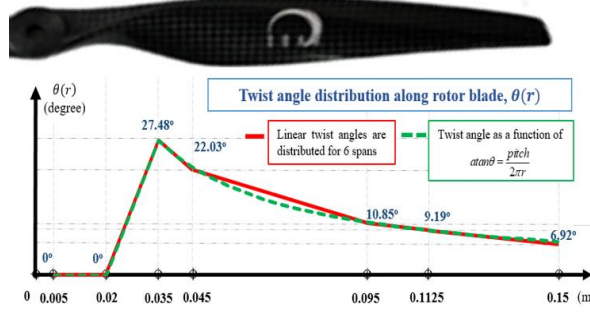$$pitch = tan\theta \times 2\pi r \qquad (1)$$

Fig 5. Twist angle distribution on the rotor blade

The rotor blade is divided into 6 segments. It assumes that the rotor characteristics considered linearized on each span section including the twist angle, chord length and local maximum thickness.

Table 1. Description of the rotor blade geometry

Modelling simplified rotor parameters						
Position (m)	r/R (%)	Twist angle (deg.)	Chord length (m)	Max. Thick-ness (m)	Ratio of thickness and chord length (%)	Airfoil typed NACA
0.005	3.33	0	0.02	-	-	-
0.020	13.3	0	0.02	0.0018	9	0012
0.035	23.3	27.4	0.02	0.0027	13.5	0012
0.045	30	22.0	0.03	0.0035	11.67	0012
0.095	63.3	10.8	0.022	0.0022	10	0012
0.115	75	9.19	0.02	0.0015	7.5	0006
0.15	100	6.92	0.015	0.001	6.67	0006

Particularly, the lift and drag coefficients are considered very important to estimate the lift force and pitching moment at each blade element. So, a local linear velocity is used to predict the local Reynold number at 6 span positions.

Table 2. Airfoil selection

Determination of Reynolds number				
Position (m)	Chord length (m)	Linear velocity (m/s)	Reynolds number	Airfoil
0.005	-	-	-	-
0.020	0.02	14.32	19 483	NACA 0012
0.035	0.022	20.03	29 976	NACA 0012
0.045	0.032	32.19	70 693	NACA 0012
0.095	0.022	67.97	101 723	NACA 0012
0.1125	0.02	80.49	109 510	NACA 0006
0.15	0.015	107.32	109 510	NACA 0006

Table 3. Reynolds number

Approximation of Reynolds number for segments			
Position(s)	r/R (%)	Airfoil(s)	Reynolds number
0.02 m	0.13	NACA 0012	Re = 20 000
0.035 m	0.23	NACA 0012	Re = 30 000
0.045 m	0.3	NACA 0012	Re = 70 000
0.095 m	0.63	NACA 0012	Re = 100 000
From 0.095 m to 0.1125 m		Blending zone	
0.1125 m	0.75	NACA 0006	Re = 110 000
0.150 m	1.0	NACA 0006	Re = 110 000

From Table 2, we choose approximately two symmetric airfoil types NACA 0012 and NACA 0006 in addition to consider the influence of the local flow at each span position (Table 3). Fig 6 shows the complete propeller typed XOAR PJP –T–L 12x45, all of the basic mentioned parameters are treated as the inputs for the rotor model.
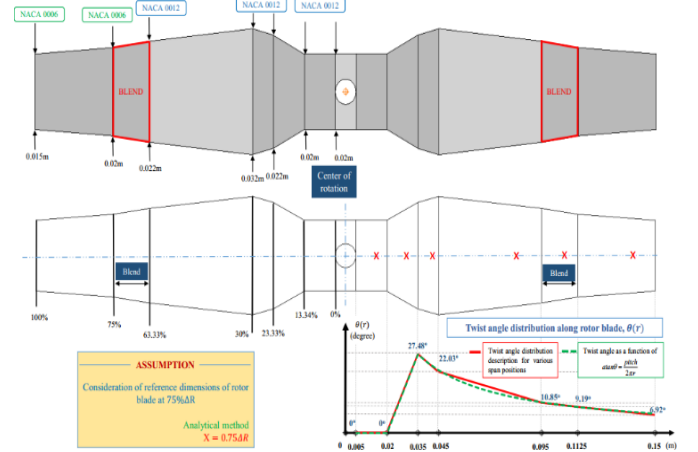

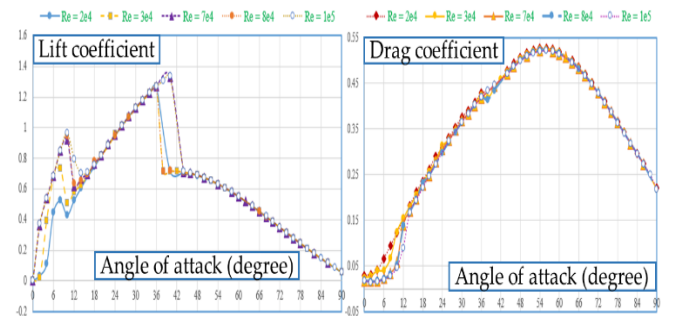Fig 6. Description of XOAR PJP-T-L 1245

Fig 7. Reynolds number on c_l and c_d

2.4 Turbulence model

In CFD simulation, choosing the turbulence model is important to get the accurate and reliable results. The k − ω SST model is a blend of the k − ε and the k – ω with some additional features of great sensitivity to the free stream values of ω whereas it behaves much better in the near wall regions than the k – ε model. (F. R. Menter, M. Kuntz , R. Langtry, 2003)

$$k = 1.5(UI)^2 = 1.5 \times (6 \times 0.02)^2 = 0.0216 \ m^2/s^2 \quad (2)$$

$$\omega = \frac{\sqrt{k}}{C_\mu^{0.25} \times l} = \frac{\sqrt{0.0216}}{0.09^{0.25} \times 0.07 \times 0.15} = 12.77 \ m/s^2 \quad (3)$$
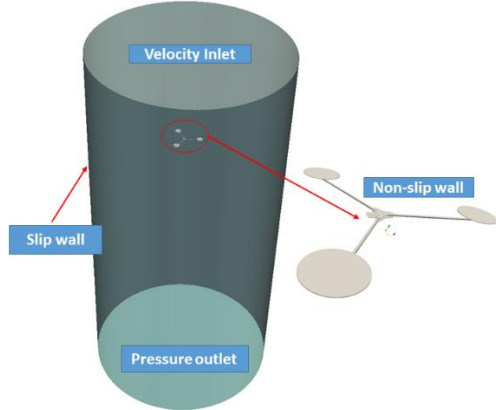
2.5 Boundary condition

Fig 8. Boundary conditions

Boundary conditions are automatically converted from Salome mesh format to OpenFOAM mesh format. A boundary file is generated by *ideasUnvToFoam* with "base type", it means BCs in *polyMesh* file formatted a basic type of *patch* or *wall* in boundary file. So, we need to assign these basic types for each of the field variables correctly as a "numerical type" (Wahono, 2013). Briefly, the BCs of numerical type are manually assigned for a series of text files in a 0 directory are summarized in

Table 4. At first, we need to understand definitions of general boundary condition types used in OpenFOAM.

The non-slip boundary condition using the wall functions can be provided near-wall boundary condition for the tricopter's surface. To be more specific, the velocity is set to zero at wall.

The slip boundary condition is applied at the walls of cylinder while the effect of viscosity on the surface is negligible.

Fixed value boundary conditions are used to describe the value of a field on boundaries such as the inlet, outlet and wall. In general, the flow velocity (*v*) is set to a fixed value corresponding to the axial climbing velocity. At the tricopter's surface (*wall*), the velocity is usually set to 0. Also, the turbulent quantities such as the turbulent kinetic energy (*k*) and the dissipation rate (*ω*) can be set to fixed values which have to be estimated first following equations (2) and (3).

Inlet-Outlet boundary condition (BC) is used at the outlet patch, which is normally the same as zeroGradient. However, the inlet-Outlet BC switches to fixedValue type if the velocity vector next to the boundary aims inside the domain (backward flow). The value of that the fixed value is the inlet value.

Table 4. Summarizing BCs for total field variables

Summary of Boundary conditions for case of climb rate Uc = 0.3 m/s					
	P	**U**	**k**	**omega**	**nut**
Internal Field	101325	(0 0 -6)	0.0216	12.77	0
Inlet	*zeroGradient*	*fixed Value*	*fixed Value*	*fixed Value*	*calculated*
Outlet	*fixed Value*	*inletOutlet*	*inletOutlet*	*inletOutlet*	*calculated*
Wall	*slip*	*slip*	*slip*	*slip*	*slip*
Tri-copter	*zeroGradient*	*fixed Value uniform (0 0 0)*	*Wall-Function*	*Wall-Function*	*Wall-Function*

3. RESULTS ANALYSIS

Table 5 summarizes the basic parameters used for the inputs in VBM module.

Table 5. A complete description of propulsion system

XOAR PJP – T – L Propeller's Characteristics			
Propeller RPM	6833		
Angular velocity (rad/s)	715.5		
VTip (m/s)	107.3		
Number of blades, B	2		
Blade radius (m)	0.15 m ~ 5.9 inch		
Hub radius (m)	0.02 m ~ 0.787 inch		
Rotor airfoil selection	NACA0012 – NACA0006 (from root to tip)		
		r/R (%)	*Taper ratio (%)*
Sectional chord length (different linear taper rates)	Increasing linear	[0.13 – 0.23]	1.10
	Decreasing linear	[0.23 – 0.30]	1.455
	Increasing linear	[0.30 – 0.63]	0.6875
	Decreasing linear	[0.63 – 0.75]	0.909
		[0.75 – 1.00]	0.75
		r/R (%)	*Twist angle (deg.)*
Twist angle distribution (different linear twist rates)	Increasing linear	[0.13 – 0.23]	[0 – 27.46]
	Decreasing linear	[0.23 – 0.30]	[27.4–22.03]
		[0.30 – 0.63]	[22.0–10.85]
		[0.63 – 0.75]	[10.85–9.2]
		[0.75 – 1.00]	[9.19–6.91]
Tip Reynolds number	110 000		

3.1 Grid convergence

In order to investigate the effect of the mesh size on the final results, we attempted to simulate two different mesh sizes named runSim1 (a fined mesh) and runSim2 (a coarse mesh) as summarized in Table 6.

Table 6. Summary of the two studied cases

Overall of final mesh quality		
	runSim1	*runSim2*
Final grid size	9.632 million	4.654 million
Hexahedral cell number	9.585 million	4.624 million
Percentage of hexahedral cell	99.51%	99.35%
Maximum aspect ratio	11.2	9.68
Maximum skewness	2.61	2.83
Average non-orthogonality mesh	6.98	7.13
Cell number of rotor disc	6524	3941
Mesh execution time	~ 14 minutes	~ 7 minutes

3.2 Residual convergence

In the runSim1 (the fined mesh), the simulation is performed for four cases of different axial climbing velocities such as 6 m/s, 2 m/s, 0.3 m/s and 0.1 m/s with the convergence criteria of 6×10^{-5}.

Table 7. Conditions for a fined mesh case

runSim1				
Flow Conditions				
Solver	simpleFoam			
Climb velocity (m/s)	-6	-2	-0.3	-0.1
Turbulence modelling	K-ω SST			
Computational Details				
Cylinder computational domain	Radius: 5m – Height: 20m			
Tricopter position	Height: 15 m ~ 590.6 in			

Fig 9 shows iteration numbers of 4 cases. V_C= 0.1 m/s, the convergence was obtained after 12000th iteration. Other cases were finished after 5000th iteration. For under relaxation factors, 0.3 was used for the pressure field. All other field factors are set to 0.5. The tip loss factor is set as the default value at 0.96.
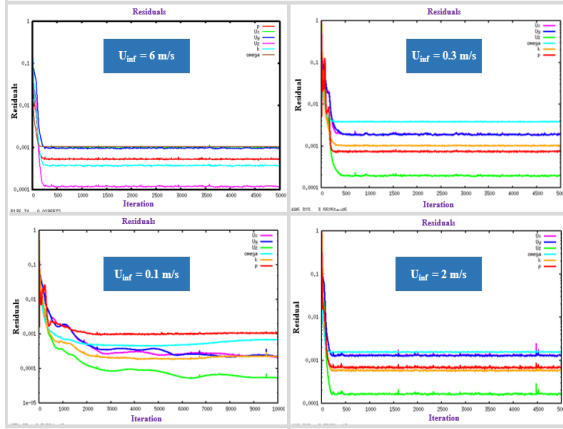
Fig 9. Residual curves of four axial climbing flights

The analytical approach using the Blade Element Momentum Theory (BEMT) is subsequently investigated to compare with the numerical approach. The BEMT is used to estimating the inflow distribution on the rotor blade. Table 8 shows a comparison of the final results for two approaches. It consists of the results from two mesh size cases as well as manufacturer's specification of PJP-T-L 1245 with 6833 revolutions per minute (RPM).

Table 8. Calculated thrust and geometric angles

Final Results From Two Studied Approaches (RPM = 6833)					
	Analytical Approach (BEMT)	Numerical Approach in OpenFOAM – (BET)			
Uc m/s		runSim1 (fined mesh)		runSim2 (coarse mesh)	
	Thrust (N)	*Error*	*Thrust (N)*	*Error*	*Thrust (N)*	*Error*
6.0	11.542	-	12.206	-	12.288	-
2.0	10.183	-	10.543	-	10.543	-
0.3	9.403	-	10.043	-	10.037	-
0.1	9.314	**12.1%**	10.012	**5.54%**	10.002	**5.64%**
Manufacturer's specifications: T = 10.6N for the propeller of RPM = 6833. *It's assumed to Uclimb = 0 m/s.*					
Uc m/s	*Geometric angles at 82% of the radius length (r ~ 0.12 m)*				
	BEMT	runSim2 (BET)	BEMT	runSim2 (BET)	
	Eff. AOA (degree)		*Inflow AOA (degree)*		

6.0	-15.03º	-18.06º	5.4º	10.2º
Δα	~ 3.03º		~ 4.8º	

Case of the climb velocity at 0.1 m/s, the total thrust generated by rotor disc in VBM module is compared with manufacturer's specification. In Table 8, the errors of the total thrust is approximately 5.6% in the numerical approach and 12% for the analytical approach calculated from the blade element momentum theory (Leishman, 2000).

Besides, the distribution of the inflow angle and the effective angle of attack on the rotor blade from two approaches are also presented in Fig 10. For example, at 82% of the radius length the effective angles there is approximately 3 degrees of difference.
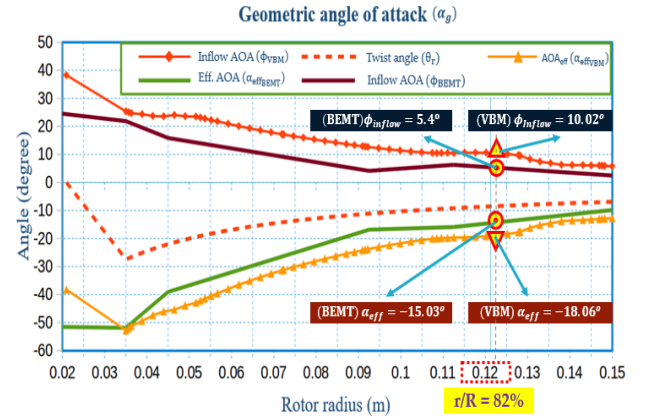

Fig 10. Distribution of angles on the rotor radius

From Table 9, the inflow angle of attack, ϕ, at every blade element is calculated from the local velocity consisting of the axial component normal to the rotor disc U_P, and the tangential component U_T parallel to the rotor disc. In this axial climbing case, the out-of-plane component (Leishman, 2000) is a combination of climb velocity (V_C) and induced velocity (V_I). At the post processing of the numerical approach, a data line in the rotor disc region is extracted to obtain the aerodynamic properties of local resultant velocities at every point along this line. Then, the relative inflow angle of attack and the effective angle of attack at the blade element are described in Table 9 with the local twist angle respectively. The inflow AOA is also called as the induced AOA as a result of induced flow.

In the BEMT's case, there are 5 linear segments corresponding to the position at 75% of each span section. The inflow angle of attack ($\phi_{BEMT} = \lambda/r_{\%}$) is distributed according to the relationship between inflow ratio (λ) and non-dimensional radial position (r).

Table 9. Geometry angle from two traditional theories

(radian)	*Blade Element Theory (VBM module)*	*Blade Element Momentum Theory (BEMT)*
Inflow AOA	$\phi_{induced} = \dfrac{U_{axial}}{U_{tangential}}$	$\phi_{induced} = \dfrac{\lambda_r}{r_{\%}}$

Effective AOA	$\alpha_{eff} = \theta_{pitch} - \phi_{induced}$

Based on the distribution of the effective angles of attack (α_{Eff}) on the radius, a look-up table of 2D aerodynamic characteristics of the airfoil type will be used for purposes of calculating the lift and pitching moment. In conclusion, the trend of inflow AOA and effective AOA (Fig 10) from two different approaches are similar.

3.3 Flow field in axial take-off flights

This section presents the flow field around the tricopter in the axial climb flight with the free-stream velocity of 6 m/s (U_C) implemented using the fined mesh – runSim1. At first, an influence of the tricopter's airframe is investigated at both positions of the tricopter's arm (under the rotor disc) and the tricopter's base by visualizing the streamlines.
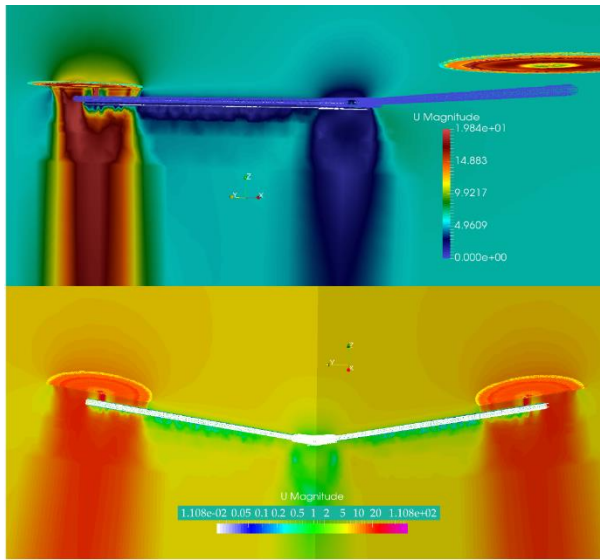
Fig 11. Velocity field around the tricopter (U_C = 6m/s)

Fig 11 shows the perturbation of the tricopter's arms on the rotor airflows when the tricopter is in the vertical flight. The velocity field below the tricopter's base and along the bottom face of the arm is approximate to 0. The tricopter is therefore considered as an obstacle to downward flows.
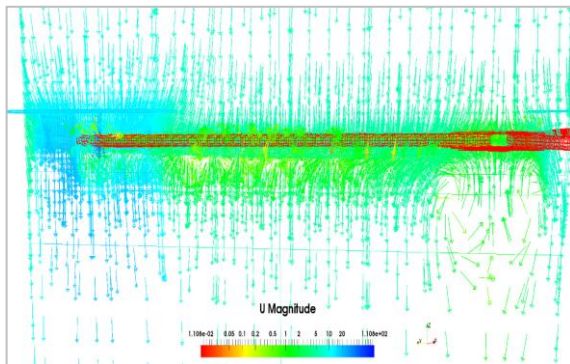
Fig 12. Flow vectors around the tricopter's arm

Fig 12 describes the direction of stream lines in the computational domain. More specifically, the change in direction of the streamlines has been shown by the directed arrows. These arrows are colored corresponding to its velocity magnitude.

For example, in the region under the tricopter's base, the streamlines tend to change direction forming a complex vortex structure. In addition, the streamlines near the rotor disc are likely to narrow its diameter just before the rotor plane (the blue zone in Fig 12).
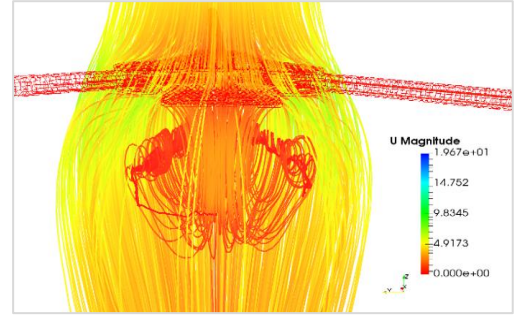

Fig 13. Circulation structure under the tricopter's base

Fig 13 shows the unstable zone of the streamlines under the base (colored red) that generates the complicated circulation patterns in the high-velocity climbing case. Clearly, Fig 14 shows the direction of the reverse flow under the tricopter's base. It describes the directional changes of arrows in a reference line at z/r = 0.5. Specifically, it's 7.5 cm away from the base and there's a difference in magnitude as well as the direction of arrows.
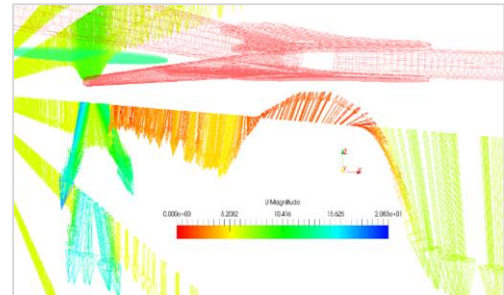

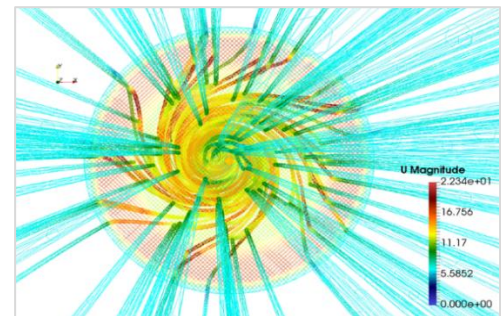Fig 14. Reverse flow structure under the tricopter's base

Fig 15. Streamlines colored by velocity magnitude (top view -wire frame mode – U_C = 6m/s)

Fig 15 shows another mode of the rotor plane that indicates the change of velocity magnitude as well as the flow direction in the right upper surface. In the range of the radial locations of 20% to 75% of rotor radius, the velocity magnitude is less than positions from 75% to 96%.

As a tip loss factor is set up at 0.96, this value is considered to be the typical setting in the simulation. It accounts for the loss of the lift at the blade tip, which corresponds up to 4% of the rotor radius from the tip blade position without lift (shown in Fig 15).

An influential investigation of the arm on the flow field is described in Fig 16. It's assumed that the rotors' reference position is placed at $z/r = 0$ (Fig 16). The rotor radius of 0.15m is used as a reference value.
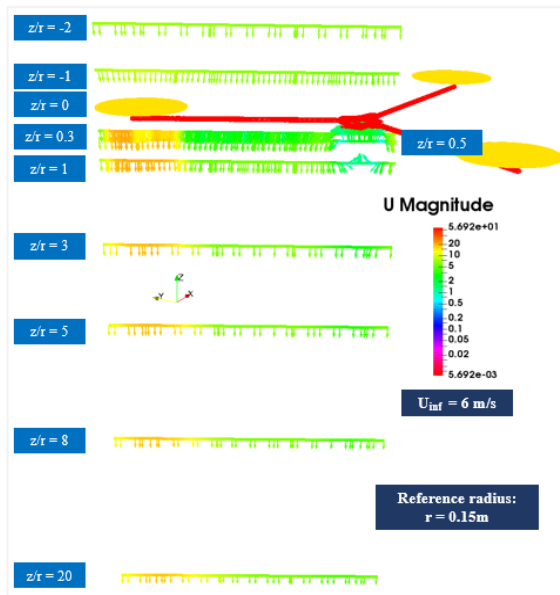
Fig 16. Reference lines parallel to the tricopter's arm (U_C = 6m/s)

Fig 16 demonstrates that the rotor's influence on reference position below rotor plane. For example, the induced flow has a large effect at $z/r=20$ – the vertical distance of 3m from rotor disc. To sum up, from reference lines described in Fig 16 and the tendency of streamlines under the base in Fig 13 and Fig 14 are shown in Fig 17. This figure describes a data extraction of each location corresponding to the points on these lines. As a result, the axial velocity components for each reference line are illustrated.

Fig 17 represents the distribution of the axial velocity components in the x coordinate of the points along the tricopter's arm length. There are 8 reference lines shown. A green dotted circle is represented the position corresponding to a rotor disc, and a red dotted circle is the position of the tricopter's base. In particular, the amber line corresponds to location $z/r = 0.33$ with the variation in velocity that is caused by the tricopter's arm. Besides, there is a group of lines with symbols. This group consists

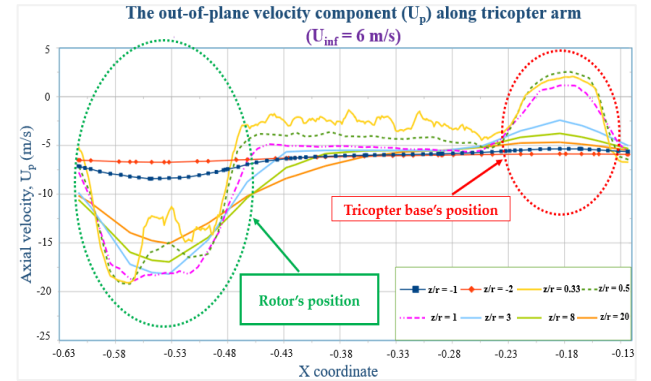of lines above placed at the distance of $1r$ (0.15 m) and $2r$ (0.3 m) from the disk plane.

Fig 17. Distribution of axial velocity of points along the direction of tricopter's arm (U_C = 6m/s)

Fig 18 shows the distribution of the dimensionless velocities (U/U_{inf}) on the non-dimensional radial positions (r/R). Where, U is the resultant local velocity on the rotor blade, U_{inf} corresponds to climbing velocity.
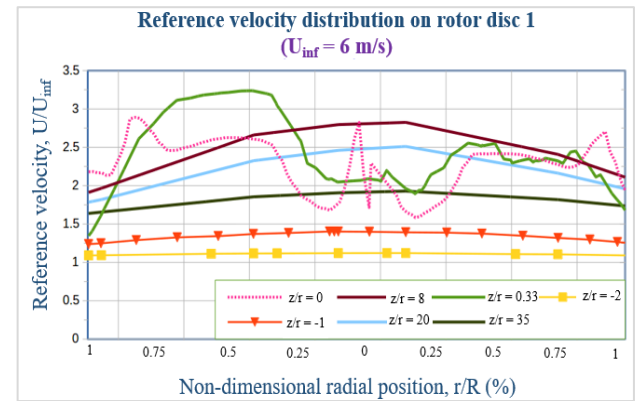

Fig 18. Distribution of dimensionless velocity on the rotor blade

As the induced airflow is under the influence of tricopter's arm placed below rotor plane, on the right rotor radius, the magnitude of velocity is smaller and non-axisymmetric.
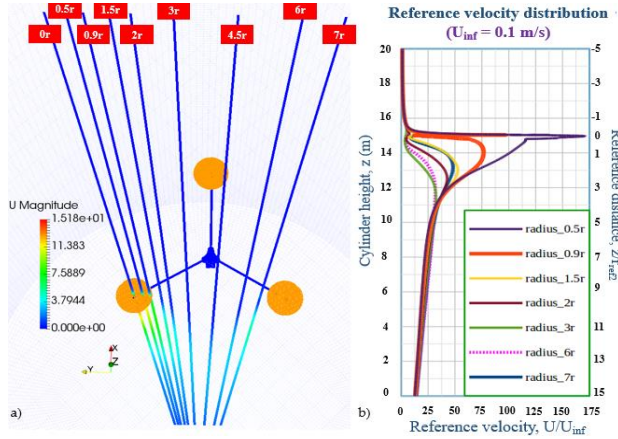
3.4 Trend of induced flow in axial climb flights

Fig 19. Induced airflow generated by the front rotor discs
($U_C = 0.1$ m/s)

In order to study the influence of the two climb modes of operation of 6 m/s and 0.1 m/s, the interaction of induced flow before and after passing through the rotor surface will be demonstrated in Fig 19 and Fig 20.

By considering dimensionless velocity of the induced and free-stream type, we can evaluate the influence of two flight conditions. For example, in the case of 6 m/s there are two trends of induced airflow distribution under the rotor disc plane from $0.5r$ to $7.36r$ due to the second propeller (at 7.36r from the first rotor hub).
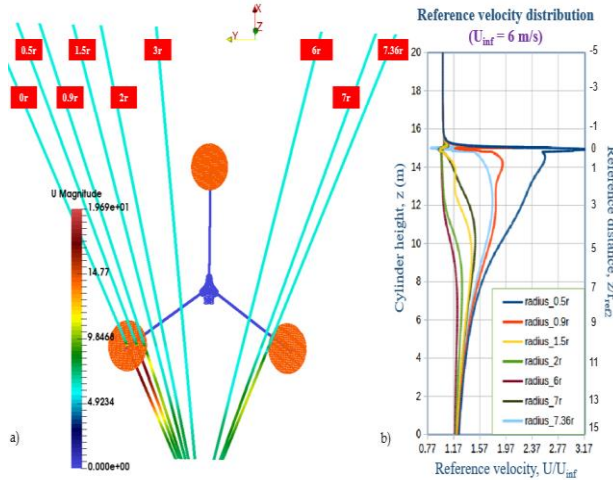

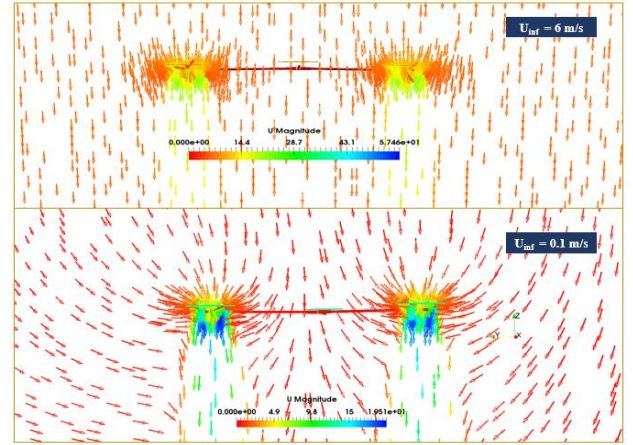Fig 20. Induced airflow generated by the front rotor discs
($U_C = 6$ m/s)

Fig 21. The streamline boundaries of the front rotor discs

Fig 21 describes the slipstream boundaries of the flow field around the rotor planes. The airflow characteristic of hover state seems similar to the case of slow vertical climbing flight $U_C = 0.1$ m/s. In other words, only one velocity is induced across the virtual blade without the free stream flow ($V_C = 0$ m/s). Fig 22 shows the stream lines colored by the velocity magnitude. The blue jade streamlines correspond to the constant free-stream velocity of 6 m/s.

It's a sudden increase of velocity when the flow is right above the rotor surface. After that is the velocity of dark-red streamlines below rotor disk plane, known as the airflow induced by propeller.
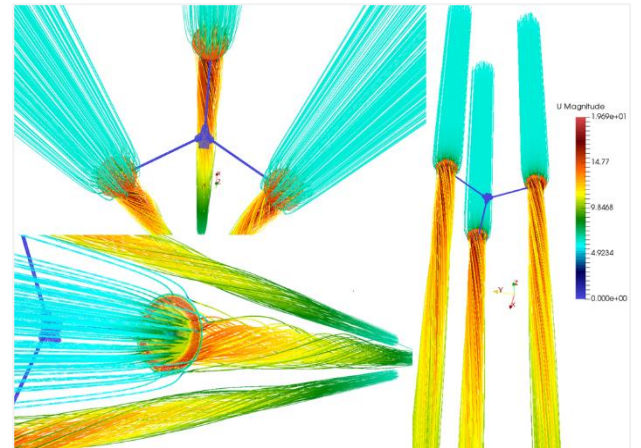

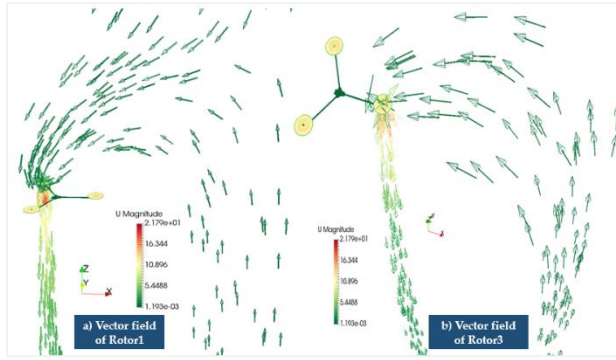Fig 22. Airflow around three rotor discs ($U_{inf} = 6$ m/s)

Fig 23. Velocity vectors into rotor disc ($U_C = 0.1$ m/s)

Fig 23 shows the velocity vectors of the inflow passing through two rotor disk positions (the front rotor disc 1 and the rear rotor disc 3). Unlike the case of climbing speeds of 6m/s. These streamlines tend to be sucked from the bottom of the computational domain onto the rotor surface of the rear rotor disc 3 and then accelerated downward. This figure describes an asymmetry streamlines passing through two rotors.

4. CONCLUSION AND RECOMMENDATION

Tricopter's simulation is implemented during the take-off state with four vertical climbing velocities at 6 m/s, 2 m/s, 0.3 m/s and 0.1 m/s, for two cases of the coarse mesh (4.5 million cell numbers) and the fined mesh (9.5 million cell numbers). The convergence criteria is set to 6×10^{-5} and the results for two mesh structures are very similar. The VBM method demonstrates the detailed streamlines, velocity field and pressure field. The interaction of the airflow induced by three rotor discs and the influence of tricopter arms to flow are then investigated. For the case of the vertical take-off velocity of 0.1 m/s, the interaction of airflow passing through three rotor discs is similar to hovering state – the rotor has zero vertical speed and zero forward speed. The flow in the bottom of the domain is drawn to the rotor disc and azimuthially axisymetric.

The results of this paper provide a methodological tool for the study of the tricopter's aerodynamic responses, especially forthe UAV-HOPE's project - a model combined between fixed wing and three rotors in certains flights such as climb, descent, hover and forward flights. However, there are some limitations of the study. Due to the numerical resources, the study could not perform the finest mesh simulations and hence could not study the influence of the rotor thickness to the lift-drag curves. Furthermore, the study also ignored the influence of the rotor hub to the free stream. These limitations will be addressed in the future.

REFERENCES

Filippone, A., Chollet, J. P., & Lewandowska, J. (2013). CFD actuator disk solutions for a helicopter rotor in hover flight. *DESS Modelisation & Simulation en Mecanique Departement Mecanique Universite, Joseph Fourier, Grenoble.*

Menter, F. R., Kuntz, M., & Langtry, R. (2003). Ten years of industrial experience with the SST turbulence model. *Turbulence, heat and mass transfer*, *4*(1), 625-632.

Leishman, G. J. (2006). *Principles of helicopter aerodynamics with CD extra*. Cambridge university press.

Sieradzki, A. (2016). Aeroelastic analysis of helicopter rotor using virtual blade model and equivalent beam model of a blade. *Journal of KONES*, *23*.

Tri, P. H. (2015). Design a vtol UAV – Control stability and Simulation analysis.

Wahono, S. (2013). *Development of Virtual Blade Model for Modelling Helicopter Rotor Downwash in OpenFOAM* (No. DSTO-TR-2931). DEFENCE SCIENCE AND TECHNOLOGY ORGANISATION FISHERMANS BEND (AUSTRALIA) AEROSPACE DIV.

PHOTOS AND INFORMATION

	Nguyen Khanh He is a student in Department of Aerospace Engineering at Ho Chi Minh city University of Technology. His current research includes Computational Fluid Dynamics (CFD) and UAV.
	Dr. Le Thi Hong Hieu She received the B.E. (2000) in Aerospace engineering from the Ho Chi Minh City University of Technology, Vietnam and the M.E. (2001), and D.E. (2005) degrees in the same major from University of Poitiers, France. She is a lecturer, Department of Aerospace Engineering, Ho Chi Minh City University of Technology. Her current interests include VTOL-UAV design and performance analysis, analytical and computational methods for wind turbines.
	Dr. Nguyen Ngoc Hien He is the lecturer at the Mathematical Science, RMIT University, Australia. He received the B.E. (2007) in Aerospace Engineering from Ho Chi Minh City University of Technology, Vietnam and Ph.D. (2013) in Computational Engineering from Singapore-MIT Alliance, Singapore. His current research of interests includes Computational Fluid Dynamics (CFD), Inverse Problems (IP), Reduced-Order Modelling (ROM), Optimal Control Problems, Machine Learning and UAV.